

Large-Area Growth of Five-Lobed and Triangular Graphene Grains on Textured Cu Substrate

Dechao Geng, Enlai Gao, Huaping Wang, Jie Xu, Zhiping Xu, and Gui Yu*

Chemical vapor deposition (CVD) has been widely employed in graphene production and integration due to its various advantages in terms of low cost, high-controllability, and high scalability.^[1–3] There usually exist striking discrepancies in the as-grown graphene when using different catalysts or gas conditions in the CVD process. Previous reports suggested that a large amount of transitional metals could be used for graphene growth.^[4–8] Among those metals, the Cu has been emerged as a particularly effective catalyst to synthesize monolayer graphene owing to ulralow carbon solubility in it.^[1] However, the carrier mobility of CVD grown graphene film on Cu foils is significantly lower than that of exfoliated graphene, most likely because of the presence of widely dispersed grain boundaries. It has been experimentally displayed that the grain boundaries are detrimental to the carrier transport properties.^[9,10] Thus the next critical step of graphene growth relies on the controlled fabrication of high-quality graphene, e.g., graphene single-crystals. Comparing with the polycrystalline film, graphene single-crystals without structural defects have posed great potential in enhancing devices performance.

Recently, several advances in growth of graphene single-crystals by CVD method have been achieved, wherein graphene crystals with several shapes have been controllably prepared.^[11–24] Among those grains, hexagonal graphene grain with high-symmetry has been the most extensively explored since it was observed on solid Cu foil.^[11] Moreover, symmetric rectangular^[12] and 12-pointed^[19] graphene grains have also been prepared. However, the growth of graphene grains with asymmetric shape has met with great challenge and achieved little success. Recently, pentagonal graphene domains were fabricated on Cu surface, where lattice steps on the crystalline surface of the underlying Cu promoted graphene growth in the direction perpendicular to the steps and finally led to

the disappearance of one of the hexagonal edges.^[25] On the one hand, the irregular shaped graphene grains have been traditionally considered to be unstable on the catalyst, which is extremely difficult to be detected. Very recent report suggested that compact five-lobed graphene can be theoretically stable in a kinetics-limited growth mechanism and displays unusual properties.^[26] On the other hand, the asymmetry is mainly attributed to the lack of a catalyst in specific directions for the unique growth. Thus, the tailoring and direct observation of novel shaped graphene grain, especially graphene with asymmetric shapes, are extremely crucial to understand the growth mechanism^[27] and to explore new properties of graphene.

Meanwhile, intensive efforts have been devoted to investigating the effects of underlying Cu substrates on the as-grown graphene during CVD process.^[28–32] It is suggested that both the initial nucleation and growth dynamics of graphene play crucial roles in determining the final quality and shape of graphene.^[33] However, such characteristics are largely dependent on Cu surface structure, suggesting that a little discrepancy in Cu processing methods has large influence on the as-grown graphene. Single-crystal Cu surfaces are ideal substrates for investigating and tailoring graphene growth in CVD process, but they are expensive and not available for growth of large-area graphene.

In this work, controlled growth of large-area five-lobed graphene grains (FLGGs) was first demonstrated by ambient pressure CVD on unique textured Cu substrate. Notably, the mild oxygenation via Ar annealing can reconstruct the crystal orientation of Cu and result in the formation of Cu (311) surface, enabling the liable growth of FLGGs. Furthermore, large-scale triangular graphene grains (TGGs) were also controllably fabricated on reconstructed Cu surface. It is concluded that the liquid textured Cu substrate can play a critical role in shaping graphene grains, more liable for growth of the asymmetric graphene. At last, a substrate-induced growth mechanism of asymmetric graphene is qualitatively proposed based on the observations. The systematical study on shape-engineering of graphene grains, especially for the asymmetric graphene, poses great potential in graphene-based science and further applications.

Our primary CH₄-CVD approach involves the growth of FLGGs on a liquid textured Cu surface in a mixture of Ar and H₂ gas at ambient pressure, as schematically shown in Figure 1a. Several pieces of Cu foils placed on W substrates were loaded into a one inch quartz tube. The tube was then heated under pure H₂ gas in a furnace to 1160 °C (above the melting point of Cu, ≈1085 °C). In the common Cu-catalyzed graphene growth, the annealing process was conducted in pure H₂ gas for reduction, enabling to remove impurities for the smooth Cu surface. However, in this case, the H₂ flux was

Dr. D. C. Geng, H. P. Wang, Dr. J. Xu, Prof. G. Yu
Beijing National Laboratory for Molecular Sciences
Institute of Chemistry
Chinese Academy of Sciences
Beijing 100190, P. R. China
E-mail: yugui@iccas.ac.cn

Dr. D. C. Geng, H. P. Wang, Dr. J. Xu, Prof. G. Yu
School of Chemistry and Chemical Engineering
University of Chinese Academy of Sciences
Beijing 10049, P. R. China

E. L. Gao, Prof. Z. P. Xu
Applied Mechanics Laboratory
Department of Engineering Mechanics and Center
for Nano and Micro Mechanics
Tsinghua University
Beijing 100084, P. R. China

DOI: 10.1002/admi.201600347



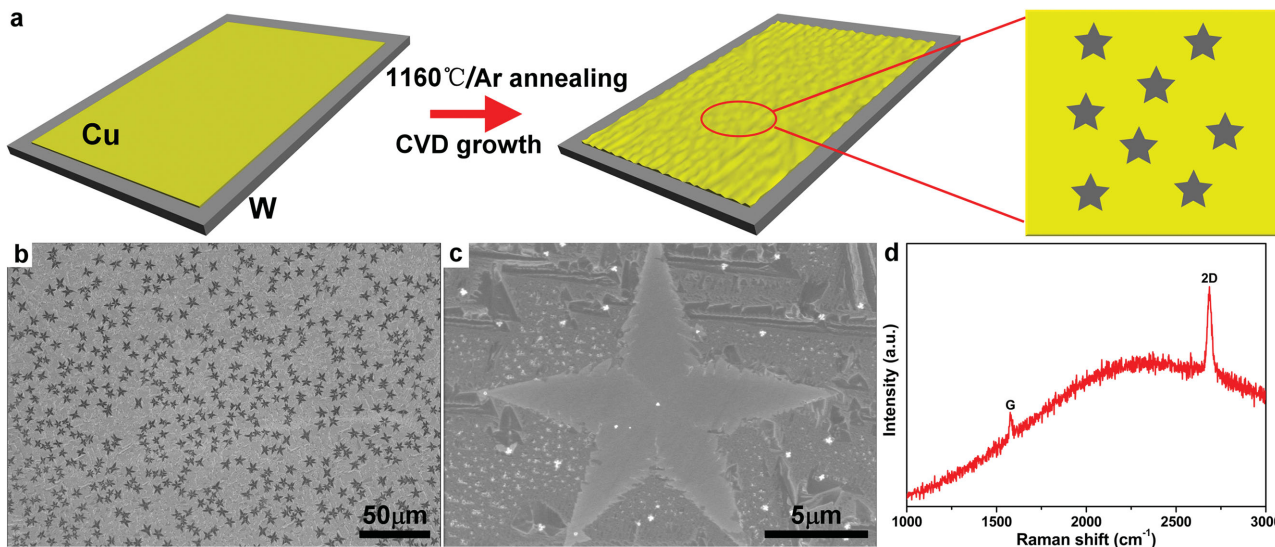


Figure 1. a) Schematic showing growth of FLGGs on textured Cu surface by CVD method. b,c) SEM images of the large-area and single FLGGs, respectively. d) Raman spectrum of FLGG on textured Cu surface, indicating the high-quality and single-layer features.

turned off and instead the samples were annealed in pure Ar gas for 30 min. The conditions of the two different annealing processes are listed in Table S1 of the Supporting Information. During the Ar annealing process, mild oxygenization of the liquid Cu takes place and then kinds of copper oxide appeared. It is properly speculated that such copper oxide can serve as a catalyst for graphene growth. After the annealing process, the CH₄ was introduced as carbon source to fabricate graphene. At the beginning of graphene growth, the 100 sccm (standard cubic centimeters per minute) Ar and 5 sccm H₂ flow rates were required, and 0.2 sccm CH₄ was then performed into the chamber for 10 min. The detailed CVD conditions are summarized in Table S2 of the Supporting Information.

Remarkably, large-scale and well-dispersed FLGGs were observed on the whole substrate as clearly shown in Figure 1b and Figure S1 of the Supporting Information under scanning electron microscopy (SEM) and optical microscopy, respectively. High-magnification SEM images further display that the structures showed fivefold asymmetry (Figure 1c) and are highly reproducible. Uniform contrast of the FLGGs with respect to the substrate is found, indicating the single-layer nature of the as-grown FLGGs (Figure S2, Supporting Information). Raman spectrum of a typical FLGG on the substrate (Figure 1d) exhibited single-layer features, in which a symmetric 2D peak located at 2698 cm⁻¹ with a full width at half-maximum of 35–40 cm⁻¹ and a large intensity ratio of the 2D and G bands ($I_{2D}/I_G = 2.5\text{--}4$). It should be noted that D peak did not detected, indicating the as-grown FLGGs have few structural defects. The distinct rough features of textured Cu substrate were detected, indicating a drastic change after exposing to Ar gas at high temperature.

Unlike the common H₂ reduction process, the pure Ar annealing resulted in striking change for the Cu structure. After the Ar annealing process, the surface of the Cu substrate goes through significant surface reconstruction at high temperatures. Optical microscopy and X-ray diffraction (XRD)

measurements were performed to probe the difference of the substrates exposed to the two annealing processes. The solid Cu surface before annealing showed a directional texture consisting of many parallel lines with spacing on the order of tens of micrometers. By adjusting the focal plane of the optical microscope, we verified that these grooves in the copper have a concave cross section. These striations are thought to be produced during the flat rolling process used to fabricate the Cu foil, with the lines running parallel to the shear/drawing direction^[34] (Figure 2a). No graphene was grown on the substrate when performing the above growth condition. Further we conducted the liquid Cu annealing in pure H₂ gas and then graphene growth as a control. It was observed that sub-millimeter sized hexagonal graphene grains were grown on liquid Cu surface (Figure 2b). As for the Cu experiencing the Ar annealing step, a clear contrast was clearly detected between the as-grown FLGGs with the underlying substrate (Figure 2c). XRD data indicated the existence of multiorientation Cu facets in solid Cu foil (Figure 2d), and then reorientated into the Cu (111) after being liquid phase in H₂ because Cu (111) facet is the energetically most stable^[35] (Figure 2e). Meanwhile, the existence of the sixfold symmetry Cu (111) facet accounts for sixfold hexagonal graphene domains.^[36–39] Nevertheless, only the Cu (311) was left after the Ar annealing (Figure 2f). The above experimental results further confirmed that the appearance of FLGGs was strongly related with the underlying liquid textured Cu. It is previously reported that the pure Ar gas annealing could largely decrease the graphene nucleation sites on Cu surface, resulting in growth of large-size graphene grains.^[40] Our experimental results further suggest its great versatility in tailoring graphene shapes.

Apart from the FLGGs, the novel four-lobed and six-lobed grains were also occasionally detected on the substrate. The typical grains are clearly shown in high-magnified SEM images (Figure 3a,b). It is found that the two kinds graphene show the highly symmetry characteristics and dendritic structure along

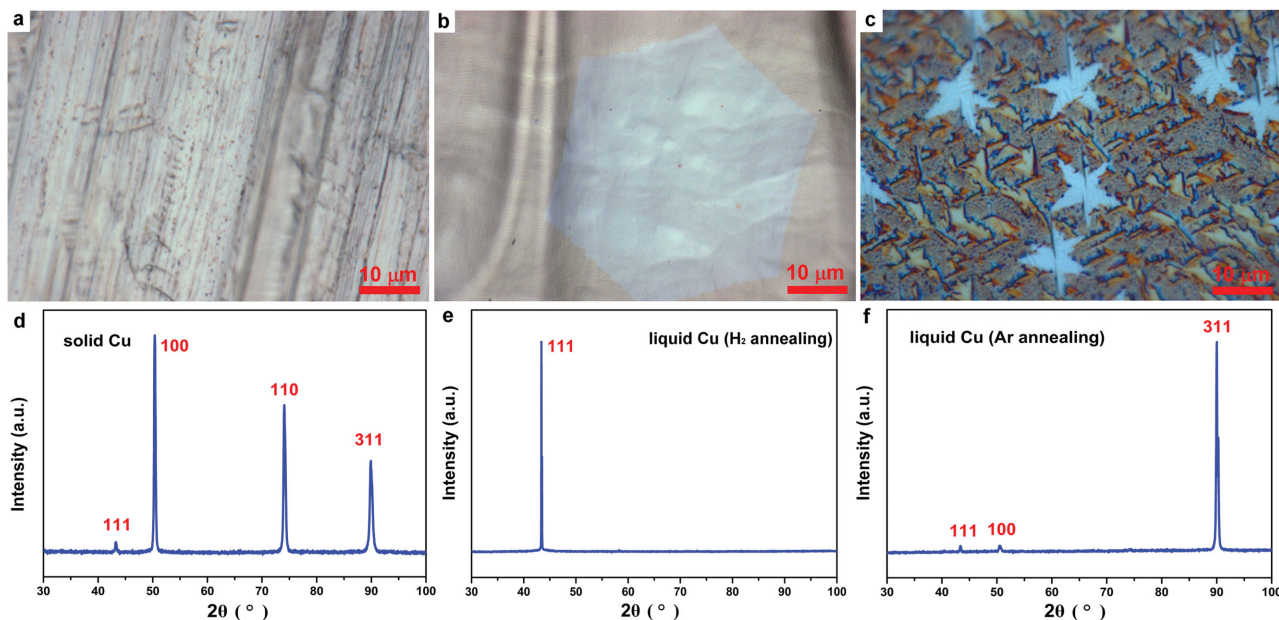


Figure 2. a–c) Optical images of the three kinds of Cu surfaces, including the solid Cu, liquid Cu, and textured Cu, respectively. c–f) The corresponding XRD measurements of the three kinds of Cu, in which the textured Cu mainly owns the Cu (311) orientation after pure Ar annealing.

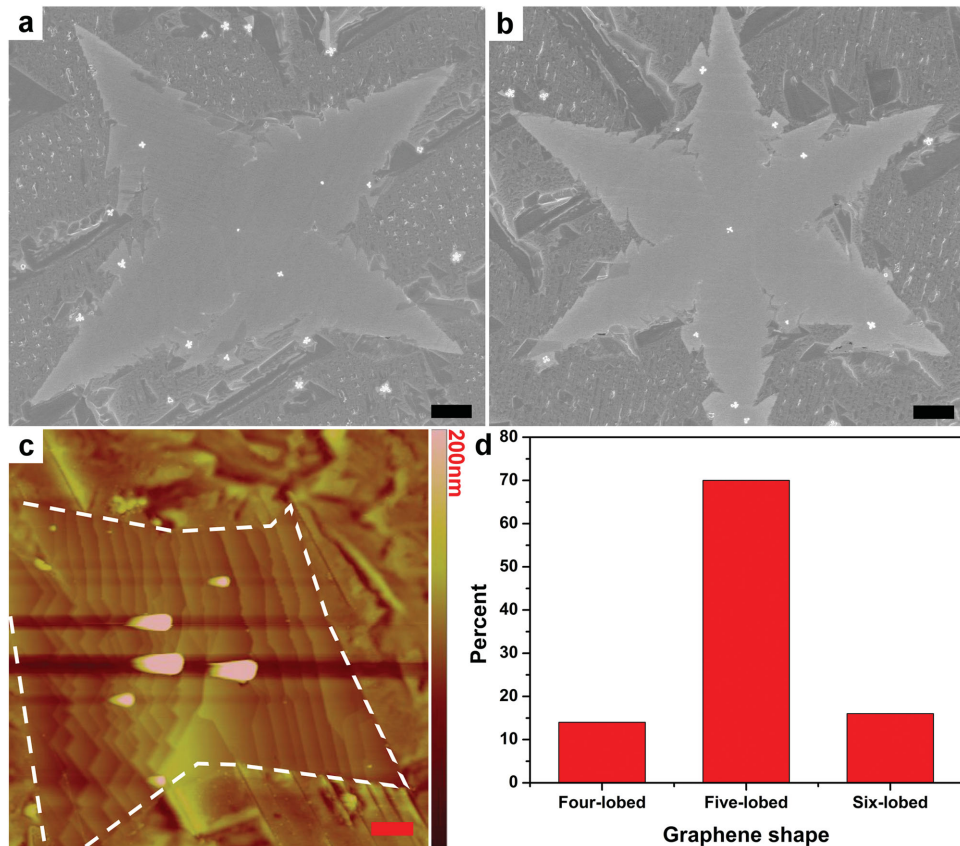


Figure 3. Characterizations of the four-lobed and six-lobed graphene flakes. a,b) SEM images of four-lobed and six-lobed graphene flakes, respectively. c) Typical AFM images of the four-lobed graphene flakes on textured Cu surface. d) Statistics of the three kind graphene flakes, clearly showing major presence of FLGGs. All the scale bars are 1 μm.

the lobes, which is caused by the existence of oxygen from Ar gas. To further investigate the as-grown lobed grains, atomic force microscopy (AFM) was performed. Figure 3c displays the four-lobed graphene grains on the textured substrate, whereas regular wrinkles were observed. It is suggested that the formation of the wrinkles are largely resulted from the discrepancy in thermal expand efficiency between graphene and substrate during the cooling process. It is properly deduced that the wrinkles can be labeled as indicator to identify the area covered with graphene or not. Statistic on counts has been conducted for the three kind grains on the same substrate, where the FLGG owns nearly seventy percent in a large portion (Figure 3d). Our experimental results further evidence that the texture Cu (311) substrate is more liable to the growth of FLGGs.

A distinct feature of the multilobed grains characterized in this work from previous reported asymmetric graphene grains^[12,19,25,26] is the appearance of dendrites, which is a clear evidence for a surface diffusion-limited growth mode. The formation of texture and low surface density of high-index (311) surface are responsible for the reduction of surface diffusivity of carbon sources. As the graphene grain is nucleated, the inhomogeneous supply of carbon to the edge reaction sites leads to shape fluctuations and shape instabilities, which is known as the point effect of diffusion.^[41] Considering the hexagonal symmetry of graphene lattice and oblique symmetry of Cu (311) surface, the shape of grain may lose hexagonal symmetry. As illustrated in Figure 4a, one or more facets (zigzag-edged) growing faster than others will disappear, resulting in nonhexagonal grains. This proposed mechanism also explains the grown graphene pentagons in a recent study.^[25] As the grain continues growing the diffusive field amplifies the shape instabilities and leads to the formation of multiple-lobe grains, where the fast-growing edges or the vertices extend out along the direction of diffusion field, i.e., the gradient of carbon source concentration. The selection of specific edges and/or vertices results in the diversity in the type of five-lobed graphene grains (Figure 4b), as well as others such as the four- and six-lobed grains. A proof of this proposed mechanisms from experimental data (Figure 1b) is that the angles between lobes are centered at 0° (60°, 120°) and 30° (90°, 150°). The angles in the parentheses are identical due to the hexagonal symmetry of graphene. The statistics shown in Figure S3 of the Supporting Information indicate that, surprisingly, not only the FLGG, but also the four- and six-lobed grains follow this rule. The dominance of FLGG in the sample is because of

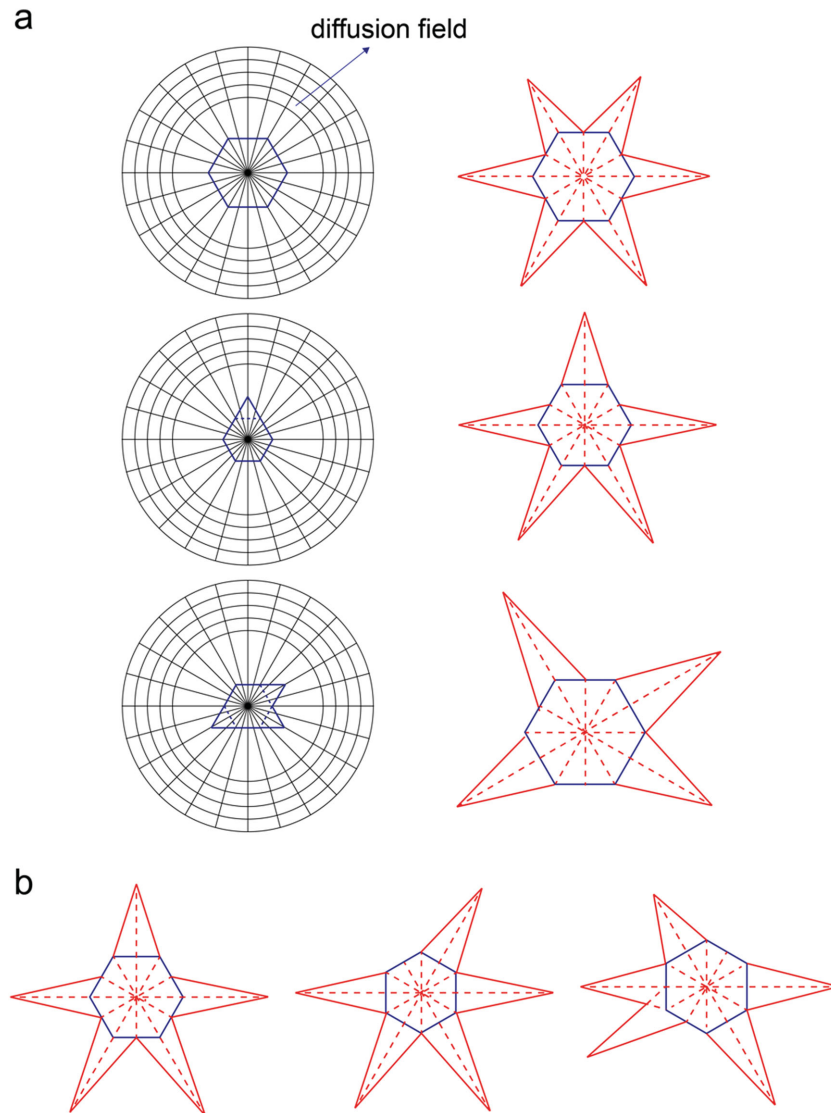


Figure 4. a) Schematics showing the mechanism of multilobe grain growth in the diffusion-limited mode. The rings are constant-concentration field of carbon sources, which defines the direction of lobe extension. The blue-colored polygons are the nucleated grains, where fluctuations could lead to instable growth. The facets could grow faster than the vertices, leading to the formation of nonhexagons. These facets and the vertices could grow fast in the diffusion-limited mode, resulting in the formation of multilobe graphene grains (red) with dendritic edge morphologies. b) Different types of five-lobed graphene grains characterized from the SEM images in Figure 1b.

the minimum fluctuation a hexagonal grain needs to lose its shape stability.

By tuning several parameters in annealing process, e.g., time, flow rate of Ar gas or even the temperature, the crystal orientation of liquid Cu substrates and even shape of graphene could be largely changed. Together with the decreased Ar flow rate (10 sccm) and annealing time (5 min), textured Cu (110) appeared instead of Cu (311). After the same growth conditions, large-area TGGs were clearly found. A combination of SEM, optical microscopy, and AFM has been conducted to probe the grains. It is shown that dendrites still exist along the as-grown TGGs, which is similar with other kind graphene

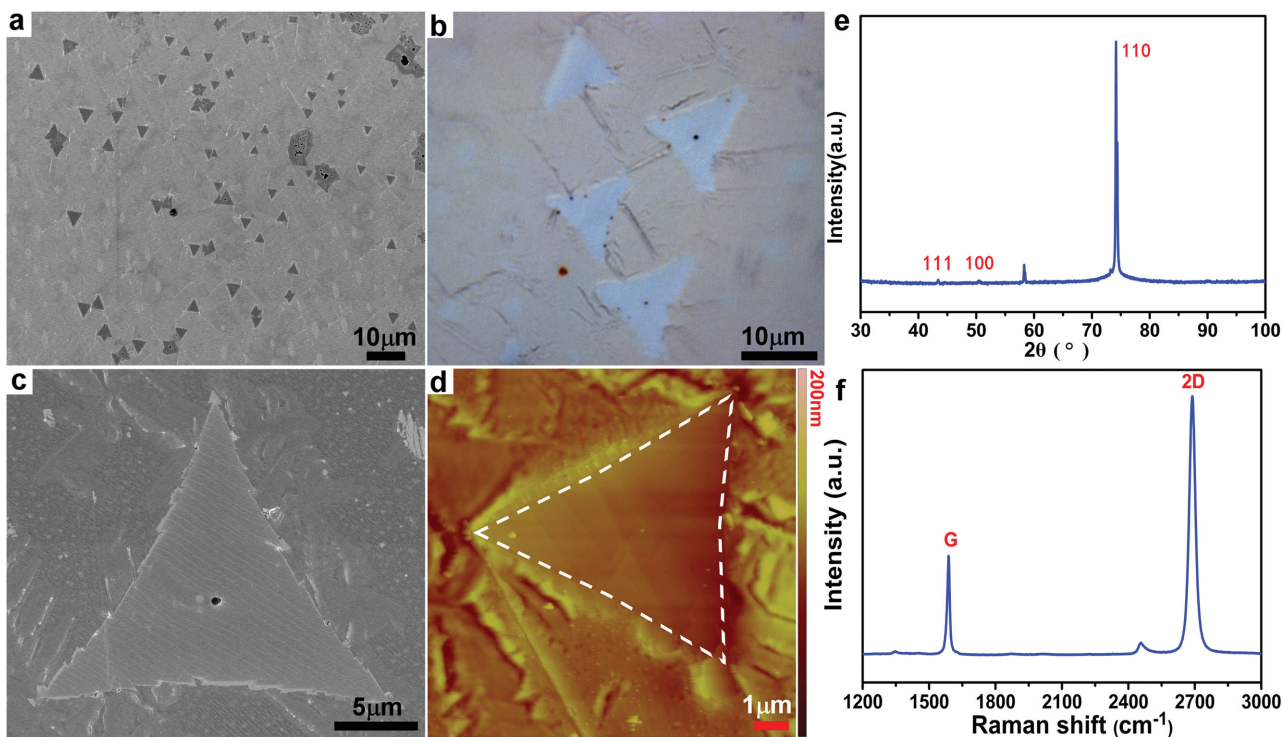


Figure 5. a,b) SEM and optical image of large-area triangle graphene flakes. c) The high-magnified SEM images of single triangle flake on textured Cu. d) AFM images of the as-grown triangle graphene flake. e) XRD measurements of the as-formed textured Cu, showing the Cu (110) orientation. f) Raman spectrum of triangle graphene flake, indicating the monolayer feature.

grains. Notably, the size of TGGs could be up to 10 μm, the largest size reported to date.

As for the large-scale grains, it is observed that the direction followed the same orientation as shown in Figure 5a. The only crystalline direction of Cu substrates was considered to be of great importance in determining the orientation. Uniform contrast of graphene with respect to the substrate was found (Figure 5b), indicating the single-layer features. A high-resolution SEM image of single TGG clearly displayed its dendritic structure along the edge (Figure 5c). A large number of parallel wrinkles were obvious on the plane which is common and characteristic in as-grown graphene on liquid Cu surface. Furthermore, AFM was conducted to verify its morphology and single layer feature (Figure 5d). Distinct change of the underlying Cu surface from pristine flat Cu can be observed, again suggesting that the patterns mostly originate from the structure of the Cu underneath the graphene. To reveal the relation between graphene shape with the substrate crystal orientation, XRD measurement was carried out (Figure 5e). Different from that in FLGG growth, polycrystalline Cu films in this case are highly textured with exposed (110) facets. Notice that, the absorption peak at about 58° attributes to exposed W since liquid Cu's incomplete wetting on W surface. Besides, Raman spectroscopy confirms the single layer feature of the TGGs (Figure 5f).

The low-index (110) surface may lead to a weaker point effect of the diffusion field and thus a more compact shape of the grown grain. Then a substrate-induced growth model is proposed for the growth of TGG. In the common case, the

solid Cu surface emerges into the liquid Cu, following the major (111) orientation in the H₂ atmosphere above 1085 °C. A thin layer close onto the Cu surface with uniform orientation can be formed (Figure 6a). Then the Ar gas is introduced into the chamber for the oxidation process, making the surface into orientated Cu (110). It is well known that metal oxides may epitaxially form on (110) oriented metals, such as Ni^[42] and Cu.^[43] It is further reported that copper oxide can be served as catalyst in fabricating graphene.^[44] It is well understood that parameters during CVD growth process can largely affect the crystallographic orientation of Cu substrate.^[45–47] Due to the presence of surface oxygen at elevated temperature (in our case at 1160 °C), the kind of CuO_x nanoparticles gradually formed. Both energy dispersive X-ray (EDX) spectroscopy (Figure S4, Supporting Information) and X-ray photoelectron spectroscopy (XPS) (Figure S5, Supporting Information) measurements confirmed the presence of Cu oxide on the substrate. Given the interact between that Cu substrate and surface oxygen together with the immigration features at the liquid phase, the CuO_x NPs can assembled into specified shape, whereas in this case the triangle shape is displayed as shown in Figure 6b and Figure S6 of the Supporting Information. Then the formation of triangular CuO_x pattern can be served as template for the growth of graphene. After the CVD growth conditions, the triangular graphene flakes are then prepared on the CuO_x patterns (Figure 6c). It should be noted that the triangular CuO_x can be clearly observed under the as-grown triangular graphene as arrowed in the SEM images, further evidencing the template effects in tuning the shape of graphene grains. Based

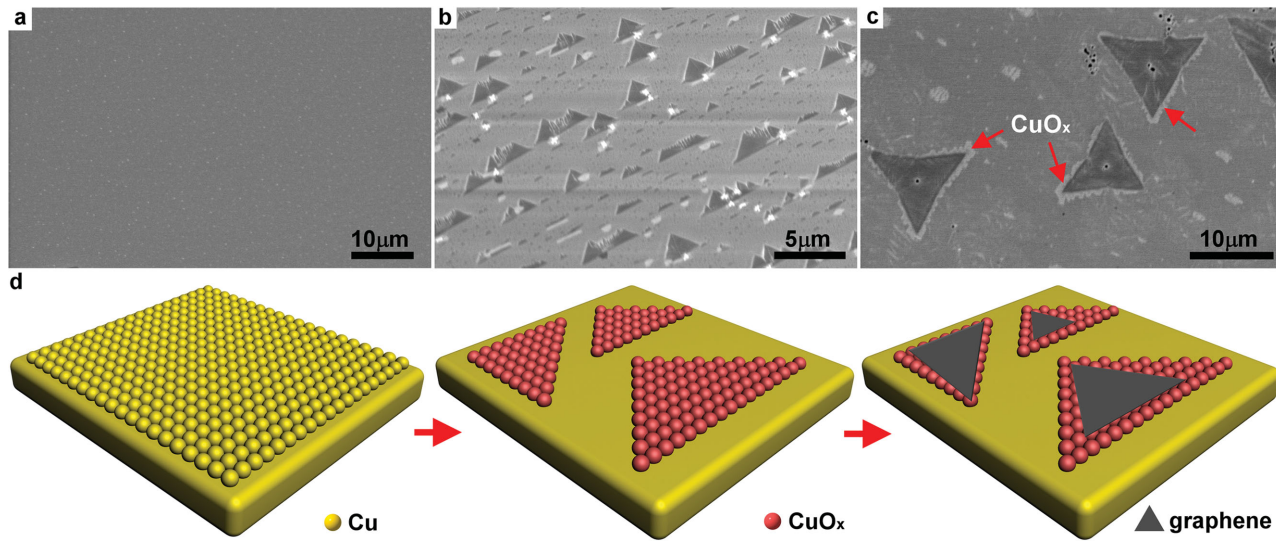


Figure 6. Growth mechanism of triangular graphene on textured Cu. a–c) SEM images of growth process of triangular graphene, in which the Cu surface can be reconstructed into specified shape after the mild oxygenation and served as template for growth of specified graphene. Notably, the template underneath graphene can be observed as arrowed in (c). d) Scheme of the whole evolution of growth of triangular graphene on textured Cu surface.

on the findings, the whole process is schematically demonstrated in Figure 6d.

In summary, we fabricate a series of graphene grains with novel shapes on textured Cu surface by chemical vapor deposition, especially the controllable growth of FLGGs, which was not reported previously. Further, the largest TGGs with the size up to tens of micrometers reported to date were prepared. Combined characterizations on the as-grown graphene and corresponding substrates structure indicated that the shape of graphene grains was strongly depended on crystal orientation of the textured Cu. The clarification on the relationship between graphene shape and copper crystal surface will shed some light on graphene growth mechanism and shape-engineering by chemical vapor deposition method. The introduction of textured Cu in graphene growth offers a facile and effective method to shape graphene via reconstructing crystal orientation of Cu surface. The controllable growth of asymmetric graphene grains can pose large potential in exploring new properties and applications of graphene.

Experimental Section

Preparation of Graphene: 50 μm thick Cu foils (99.8% purity) and 100 μm thick W foils (99.95%) purchased from Alfa Aesar were used for graphene growth. Typically, one piece of Cu foil was directly placed on a W foil before they were loaded into a horizontal silica tube mounted inside a high-temperature furnace. The CVD system was evacuated and back-filled with Ar and H₂ three times to remove air. Then the tube in furnace was heated to 1160 °C for 40–50 min under 300 sccm H₂. Prior to graphene growth, annealing treatment was performed in Ar gas under desired flow rate for certain time. During the graphene growth, a mixture of CH₄ and H₂ were introduced to the chamber, and the flow rate of Ar gas was tuned to a proper value. When the growth finished, CH₄ and H₂ were shut off and the system was rapidly cooled to room temperature under pure Ar.

SEM images were obtained using a Hitachi S-4800 scanning electron microscope. Optical images were recorded by an optical microscopy

(Olympus BX51). AFM images were obtained using a Vecco NanoMan VS microscope in the tapping mode. Raman spectra were performed using a Renishaw Invia plus with laser excitation of 514 nm and spot size of 1–2 μm. XRD measurements were performed on a PANalytical X’Pert PRO instrument with Cu K α radiation. XPS were conducted on ESCALab220i-XL instrument.

Supporting Information

Supporting Information is available from the Wiley Online Library or from the author.

Acknowledgements

This work was supported by the National Natural Science Foundation of China (61390502), the National Major State Basic Research Development Program (2013CB933403 and 2013CBA01602), and the Strategic Priority Research Program of the Chinese Academy of Sciences (XDB 12030100).

Received: April 26, 2016

Revised: July 19, 2016

Published online: August 11, 2016

- [1] X. S. Li, W. W. Cai, J. H. An, S. Kim, J. Nah, D. X. Yang, R. D. Piner, A. Velamakanni, I. Jung, E. Tutuc, S. K. Banerjee, L. Colombo, R. S. Ruoff, *Science* **2009**, *324*, 1312.
- [2] A. Reina, X. T. Jia, J. Ho, D. Nezich, H. B. Son, V. Bulovic, M. S. Dresselhaus, J. Kong, *Nano Lett.* **2009**, *9*, 30.
- [3] K. S. Kim, Y. Zhao, H. Jang, S. Y. Lee, J. M. Kim, K. S. Kim, J. H. Ahn, P. Kim, J. Y. Choi, B. H. Hong, *Nature* **2009**, *457*, 706.
- [4] Y. Z. Xue, B. Wu, Y. L. Guo, L. P. Huang, L. Jiang, J. Y. Chen, D. C. Geng, Y. Q. Liu, W. P. Hu, G. Yu, *Nano Res.* **2011**, *4*, 1208.
- [5] E. A. Sutter, P. Albrecht, P. W. Sutter, *Appl. Phys. Lett.* **2009**, *95*, 133109.

- [6] M. E. Ramon, A. Gupta, C. Corbet, D. A. Ferrer, H. C. P. Mowva, G. Carpenter, L. Colombo, G. Bourianoff, M. Doczy, D. Akinwande, E. Tutuc, S. K. Banerjee, *ACS Nano* **2011**, *5*, 7198.
- [7] K. S. Kim, Y. Zhao, H. Jang, S. Y. Lee, J. M. Kim, K. S. Kim, J.-H. Ahn, P. Kim, J.-Y. Choi, B. H. Hong, *Nature* **2009**, *5*, 457.
- [8] T. Ozbuluer, E. Pince, E. O. Polat, O. Balci, O. Salihoglu, C. Kocabas, *Appl. Phys. Lett.* **2011**, *98*, 183101.
- [9] K. Kim, Z. Lee, W. Regan, C. Kisielowski, M. F. Crommie, A. Zettl, *ACS Nano* **2011**, *5*, 2142.
- [10] P. Y. Huang, C. S. Ruiz-Vargas, A. M. van der Zande, W. S. Whitney, M. P. Levendorf, J. W. Kivek, S. Garg, J. S. Alden, C. J. Hustedt, Y. Zhu, J. Park, P. L. McEuen, D. A. Muller, *Nature* **2011**, *469*, 389.
- [11] B. Wu, D. C. Geng, Y. L. Guo, L. P. Huang, Y. Z. Xue, J. Zheng, J. Y. Chen, G. Yu, Y. Q. Liu, L. Jiang, W. P. Hu, *Adv. Mater.* **2011**, *23*, 3522.
- [12] G. P. Dai, M. H. Wu, D. K. Taylor, K. Vinodgopal, *Mater. Res. Lett.* **2013**, *2*, 67.
- [13] J. W. Liu, J. Wu, C. M. Edwards, C. L. Berrie, D. Moore, Z. J. Chen, V. A. Maroni, M. P. Panthanaman, A. Goyal, *Adv. Funct. Mater.* **2011**, *21*, 3868.
- [14] D. C. Geng, B. Wu, Y. L. Guo, L. P. Huang, Y. Z. Xue, J. Y. Chen, G. Yu, L. Jiang, W. P. Hu, Y. Q. Liu, *Proc. Natl. Acad. Sci. USA* **2012**, *109*, 7992.
- [15] A. W. Robertson, J. H. Warner, *Nano Lett.* **2011**, *11*, 1182.
- [16] I. Vlassiouk, M. Regmi, P. Fulvio, S. Dai, P. Datskos, G. Eres, S. Smirnov, *ACS Nano* **2011**, *5*, 6069.
- [17] Q. K. Yu, L. A. Jauregui, W. Wu, R. Colby, J. Tian, Z. H. Su, H. Cao, Z. Liu, D. Pandey, D. Wei, T. F. Chung, P. Peng, N. P. Guisinger, E. A. Stach, J. Bao, S. S. Pei, Y. P. Chen, *Nat. Mater.* **2011**, *10*, 443.
- [18] X. S. Li, C. W. Magnuson, A. Venugopal, R. M. Tromp, J. B. Hannon, E. M. Vogel, L. Colombo, R. S. Ruoff, *J. Am. Chem. Soc.* **2011**, *133*, 2816.
- [19] D. C. Geng, L. Meng, B. Y. Chen, E. L. Gao, W. Yan, H. Yan, B. R. Luo, J. Xu, H. P. Wang, Z. P. Mao, Z. P. Xu, L. He, Z. Y. Zhang, L. M. Peng, G. Yu, *Adv. Mater.* **2015**, *26*, 6423.
- [20] Y. A. Wu, A. W. Robertson, F. Schäffel, S. C. Speller, J. H. Warner, *Chem. Mater.* **2011**, *23*, 4543.
- [21] H. Ago, I. Tanaka, C. M. Orofeo, M. Tsuji, K. Ikeda, *Small* **2010**, *6*, 1226.
- [22] H. Wang, G. Z. Wang, P. F. Bao, S. L. Yang, W. Zhu, X. Xie, W. J. Zhang, *J. Am. Chem. Soc.* **2012**, *134*, 3627.
- [23] J. M. Wofford, S. Nie, K. F. McCarty, N. C. Bartelt, O. D. Dubon, *Nano Lett.* **2010**, *12*, 4890.
- [24] M. Massicotte, V. Yu, E. Whiteway, D. Vatnik, M. Hilke, *Nanotechnology* **2013**, *24*, 325601.
- [25] K. L. Xia, V. I. Artyukhov, L. F. Sun, J. Y. Zheng, L. Y. Jiao, B. I. Yakobson, Y. Y. Zhang, *Nano Res.* **2016**, *9*, 2182.
- [26] S. H. Zhang, J. Zhou, Q. Wang, X. S. Chen, Y. Kawazo, P. Jena, *Proc. Natl. Acad. Sci. USA* **2015**, *112*, 2372.
- [27] J. Akola, H. P. Heiskanen, M. Manninen, *Phys. Rev. B* **2008**, *77*, 193410.
- [28] Z. Y. Zhang, M. G. Lagally, *Science* **1997**, *276*, 377.
- [29] J. D. Wood, S. W. Schmucker, A. S. Lyons, E. Pop, J. W. Lyding, *Nano Lett.* **2011**, *11*, 4547.
- [30] W. H. Zhang, P. Wu, Z. Y. Li, J. L. Yang, *J. Phys. Chem. C* **2011**, *115*, 17782.
- [31] X. Mi, V. Meunier, N. Koratkar, Y. F. Shi, *Phys. Rev. B* **2012**, *85*, 155436.
- [32] E. Meca, J. Lowengrub, H. Kim, C. Mattevi, V. B. Shenoy, *Nano Lett.* **2013**, *13*, 5692.
- [33] H. Kim, C. Mattevi, M. R. Calvo, J. C. Oberg, L. Artiglia, S. Agnoli, C. F. Hirjibehedin, M. Chhowalla, E. Saiz, *ACS Nano* **2012**, *4*, 3614.
- [34] J. Hirsch, K. Lucke, *Acta Metall.* **1988**, *36*, 2863.
- [35] D. Chatain, V. Ghetta, P. Wynblatt, *Interface Sci.* **2004**, *12*, 7.
- [36] R. M. Jacobberger, M. S. Arnold, *Chem. Mater.* **2013**, *25*, 871.
- [37] S. Nie, J. M. Wofford, N. C. Bartelt, O. D. Dubon, K. F. McCarty, *Phys. Rev. B* **2011**, *84*, 155425.
- [38] A. T. Murdock, A. Koos, T. B. Britton, L. Houben, T. Batten, T. Zhang, A. J. Wilkinson, R. E. Dunin-Borkowski, C. E. Lekka, N. Grobert, *ACS Nano* **2013**, *7*, 1351.
- [39] Y. Zhang, L. Zhang, P. Kim, M. Ge, Z. Li, C. Zhou, *Nano Lett.* **2012**, *12*, 2810.
- [40] L. Gan, Z. T. Luo, *ACS Nano* **2013**, *10*, 9480.
- [41] T. Michely, J. Krug, *Islands, Mounds, and Atoms: Patterns and Processes in Crystal Growth Far from Equilibrium*, Springer, Berlin **2004**.
- [42] T. G. Woodcock, J. S. Abell, J. Eickemeyer, B. Holzapfel, *J. Microsc. Oxford* **2004**, *216*, 123.
- [43] J. C. Yang, B. Kolasa, J. M. Gibson, M. Yeadon, *Appl. Phys. Lett.* **1998**, *73*, 2841.
- [44] S. Gottardi, K. Müller, L. Bignardi, J. C. Moreno-López, T. A. Pham, O. Ivashenko, M. Yablonskikh, A. Barinov, J. Björk, P. Rudolf, M. Stöhr, *Nano Lett.* **2015**, *15*, 917.
- [45] C. W. Magnuson, X. H. Kong, H. X. Ji, C. Tan, H. F. Li, R. Piner, C. A. Ventrice Jr., R. S. Ruoff, *J. Mater. Res.* **2014**, *29*, 403.
- [46] Z. Luo, Y. Lu, D. W. Singer, M. E. Berck, L. A. Somers, B. R. Goldsmith, A. T. C. Johnson, *Chem. Mater.* **2011**, *23*, 1441.
- [47] J. D. Wood, S. W. Schmucker, A. S. Lyons, E. Pop, J. W. Lyding, *Nano Lett.* **2011**, *11*, 4547.

Copyright WILEY-VCH Verlag GmbH & Co. KGaA, 69469 Weinheim, Germany, 2016.



Supporting Information

for *Adv. Mater. Interfaces*, DOI: 10.1002/admi.201600347

Large-Area Growth of Five-Lobed and Triangular Graphene Grains on Textured Cu Substrate

*Dechao Geng, Enlai Gao, Huaping Wang, Jie Xu, Zhiping Xu,
and Gui Yu**

Supporting information

Large-Area Growth of Five-Lobed and Triangular Graphene Grains on Textured Cu Substrate

Dechao Geng, Enlai Gao, Huaping Wang, Jie Xu, Zhiping Xu, and Gui Yu*

[*] Prof. G. Yu, D. C. Geng, H. P. Wang, J. Xu

Beijing National Laboratory for Molecular Sciences, Institute of Chemistry, Chinese Academy of Sciences, Beijing 100190, P. R. China

E-mail: yugui@iccas.ac.cn

Prof. G. Yu, D. C. Geng, H. P. Wang, J. Xu

University of Chinese Academy of Sciences, Beijing 10049, P. R. China

Prof. Z. P. Xu, E. L. Gao

Applied Mechanics Laboratory, Department of Engineering Mechanics and Center for Nano and Micro Mechanics, Tsinghua University, Beijing 100084, P. R. China

Methods:

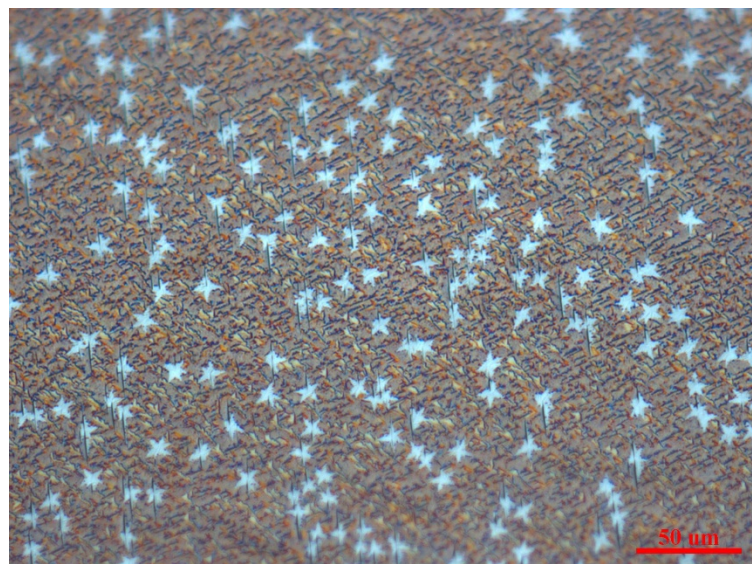
Several pieces of Cu foils were placed on the W substrate. After samples were put into the 1 inch quartz tube, the whole system was pumped to ~5 Pa followed by filling the system with H₂. After switching off pumping, the quartz tube is at an ambient pressure with continuous H₂ flow. The furnace was then heated up to a fixed temperature in ~1 h followed by annealing process. Pure H₂ and pure Ar gas are introduced during the annealing stage, respectively. Different annealing conditions as listed in Table S1 can allow reconstruction of Cu surface and thus lead to the formation of graphene with different shapes. FLGGs and TGGs were transferred to a 300 nm SiO₂/Si substrate by electrochemical method.

Table S1. Summary of annealing conditions in pure H₂ and pure Ar gas, respectively.

Annealing type	Temperature (°C)	CH ₄ (sccm)	Ar (sccm)	H ₂ (sccm)	Time (min)
Pure H₂	1160	0	0	300	30
Pure Ar	1160	0	100	0	30

Table S2. CVD growth conditons of FLGGs and TGGs.

Graphene type	Stage	Temperature (°C)	CH ₄ (sccm)	Ar (sccm)	H ₂ (sccm)	Time (min)
FLGGs	Annealing	1160	0	300	0	30
	Growth	1160	0.2	100	5	10
TGGs	Annealing	1160	0	10	0	5
	Growth	1160	0.2	100	5	10

**Figure S1.** Optical image of large-area FLGGs on textured Cu surface, indicating a high reproducibility.

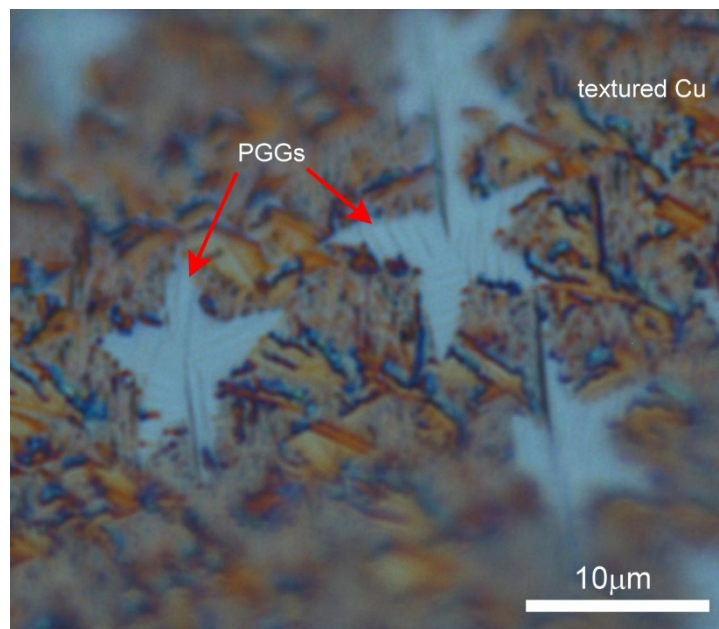


Figure S2. Uniform color contrast of FLGGs with respect to textured Cu substrate under optical microscopy.

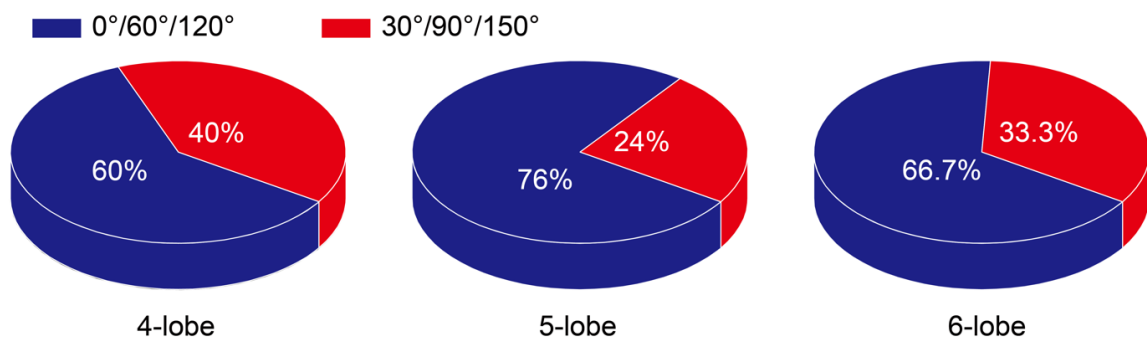


Figure S3. Statistics of the inter-lobe angles for four-, five-, and six-lobed graphene grains.

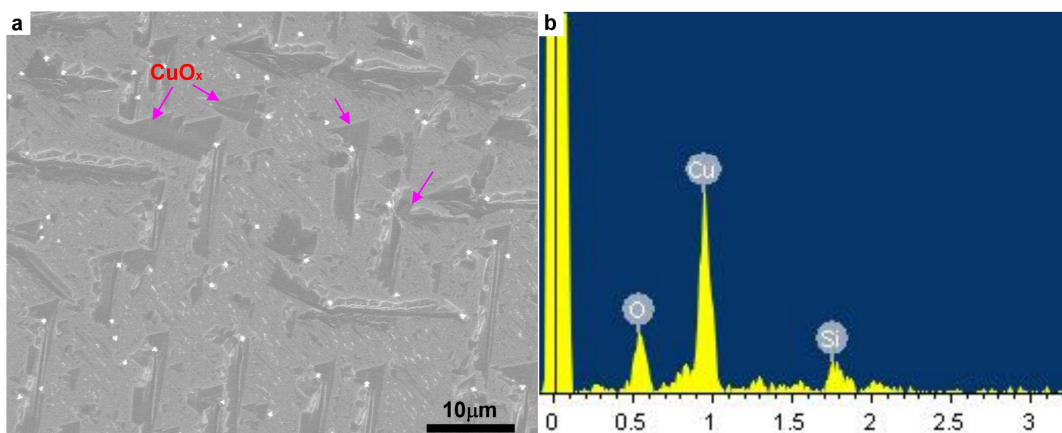


Figure S4. Determination of CuO_x on the substrate. (a) SEM image of the as-formed triangular CuO_x . (b) EDX result of the area marked in (a), indicating the presence of CuO_x .

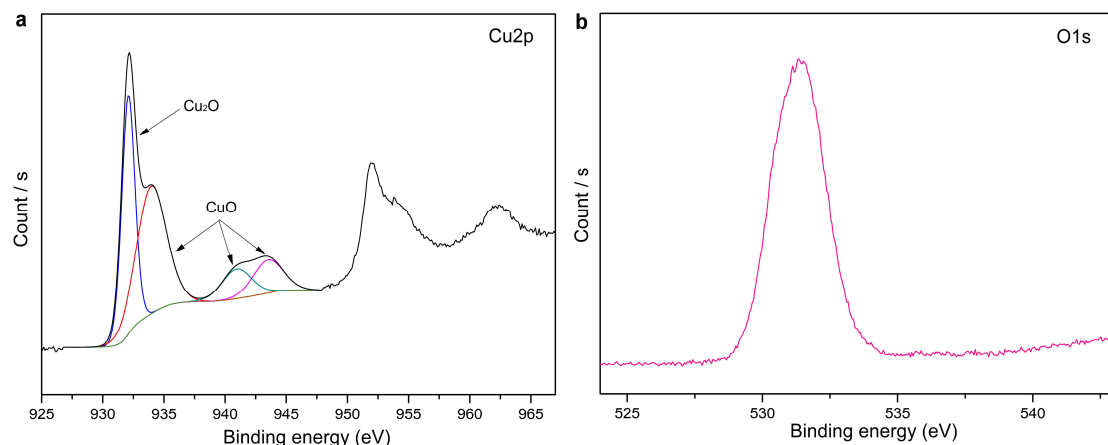


Figure S5. XPS measurements of the as-formed CuO_x . (a and b) The signals of Cu and O, respectively.

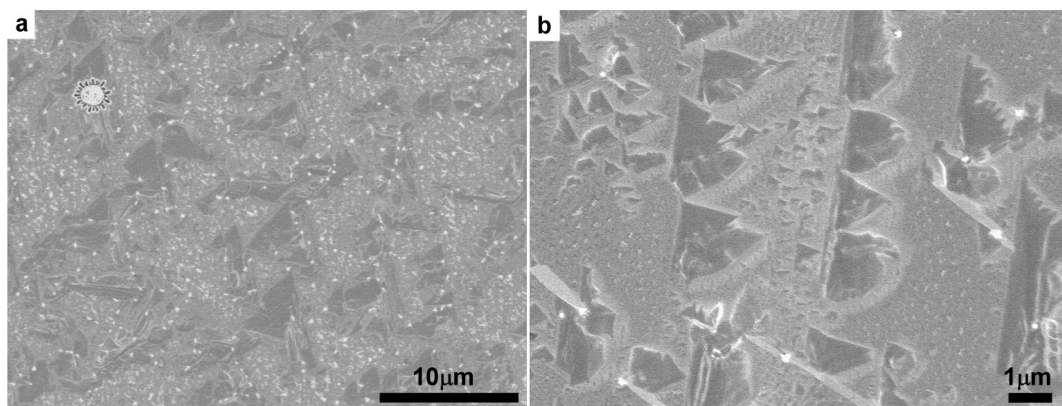


Figure S6. SEM images of the as-formed CuO_x , where the triangular shaped CuO_x have been observed on the surface.